MRS Communications

https://doi.org/10.1557/s43579-024-00597-6

MRS Communications

Early Career Distinguished Presenter Prospective

Progress and prospects of quantum emission from perovskites

Arka Chatterjee, Sadie Brasel, and Autumn Bruncz, Department of Electrical and Computer Engineering, Rice University, Houston, TX 77005, USA
Wenjing Wu, Department of Electrical and Computer Engineering, Rice University, Houston, TX 77005, USA; Applied Physics Graduate Program, Smalley-Curl Institute, Rice University, Houston, TX 77005, USA
Shengxi Huang, Department of Electrical and Computer Engineering, Rice University, Houston, TX 77005, USA

Address all correspondence to Shengxi Huang at **Shengxi.Huang@rice.edu**

(Received 6 March 2024; accepted 13 June 2024)

Abstract

Quantum emissions, such as single photon emission (SPE) and superradiance (SR), are fundamental ingredients of quantum optical technology. The quest for efficient, controllable, and scalable quantum emitters is crucial for successfully implementing various quantum technologies, such as quantum computing, secure quantum communication and high-precision metrology. Recently, perovskite quantum dots (PQDs) have emerged as highly efficient sources of quantum emission due to their excellent optical properties, including near 100% quantum yield, high optical absorbance, and tunable bandgaps covering the entire visible range. This Prospective introduces the principles of quantum emissions, including SPE and SR, and summarizes recent progress in exploring quantum emissions in PQDs. We focus on the prospects, advantages, and challenges associated with the quantum emissions from PQDs. This Prospective concludes with an outlook on PQDs in advancing future quantum technologies.

Introduction

Quantum emission serves as a foundational element for developing and advancing quantum technologies with applications ranging from secure communication to powerful quantum computation and high-precision metrology.[1–4] SPE and SR stand as two important pillars within the domain of quantum emission. SPE refers to the emission of one photon at a time into a specific spatiotemporal mode, where all emitted photons are identical. On the other hand, when a group of emitters interact coherently through a shared light field, their collective behavior can diverge significantly from that of individual constituents. Following the coherent excitation of such an ensemble, the collective coupling leads to a many-body quantum phenomenon known as SR, resulting in brief and intense bursts of light. This collective emission of photons is one of the most remarkable demonstrations of quantum optical effects, which was proposed theoretically for the first time in a seminal paper by Dicke (1954).[5]

The search for optimal quantum emitters has driven researchers to study a broad range of materials in the past. Until now, scientists have found SPEs in materials of different dimensions: zero-dimensional materials, such as GaAs and InAs QDs[6,7]; one-dimensional materials, such as carbon nanotubes and InP nanowires[8]; two-dimensional (2D) materials, such as hexagonal boron nitride (hBN) and transition metal dichalcogenides (TMDs)[9,10] and three-dimensional (3D) materials, such as diamond and GaN.[11] SR has also been observed in a couple of physical systems, including molecular aggregates and crystals,[12] nitrogen-vacancy centers in diamonds,[13] and epitaxially grown QDs.[14] In both SPE and SR, optical properties such as brightness, quantum yield, spectral linewidth, and stability are key metrics.

Most recently, halide PQDs have emerged as a distinctive class of quantum emitters, characterized by their impressive optical properties such as remarkably high photoluminescence quantum yield (PLQY) near 100%, sharp and bright PL, and tunable bandgaps spanning the entire visible spectrum (Fig. 1).[15,16] In the last few years, several reports have been published on the SPE and SR properties of perovskite nanocrystals (NCs) and QDs, proving them to be unique candidates for quantum emission.[17,18] Therefore, it is necessary to summarize and outline the single-photon and superradiant emission from colloidal PQDs and discuss recent advances in this emerging field.

Herein, we introduce the detailed background and mechanism of the SPE and SR. The structure, optical properties, and a brief outline of synthesis procedures are discussed. Recent advancements, challenges, and prospects in this field are also addressed.

An overview of single photon emission and superradiance

Single photon emission

Single photons represent individual excitations of electromagnetic field modes, acting as solutions to Maxwell's equations.[19] Their versatility is evident in metrology, quantum computing, imaging, and quantum communication applications.[20,21] The state characterizes an ideal single photon $|1_k$, where k specifies the field mode in which the photon resides.

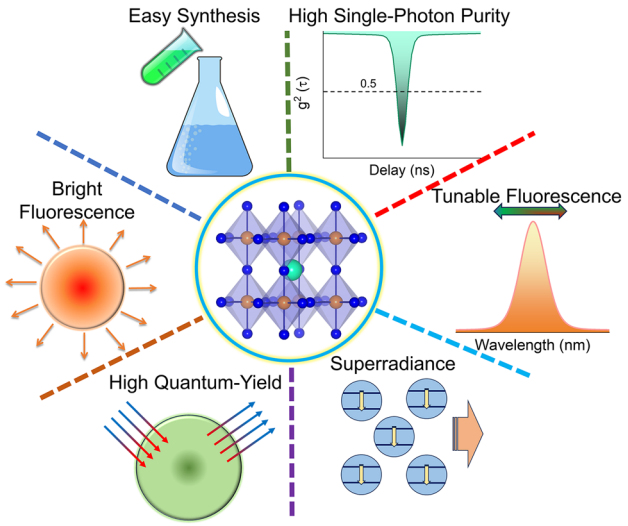

Figure 1. Schematic representation showcasing the unique features of PQDs as an efficient source of quantum emission.

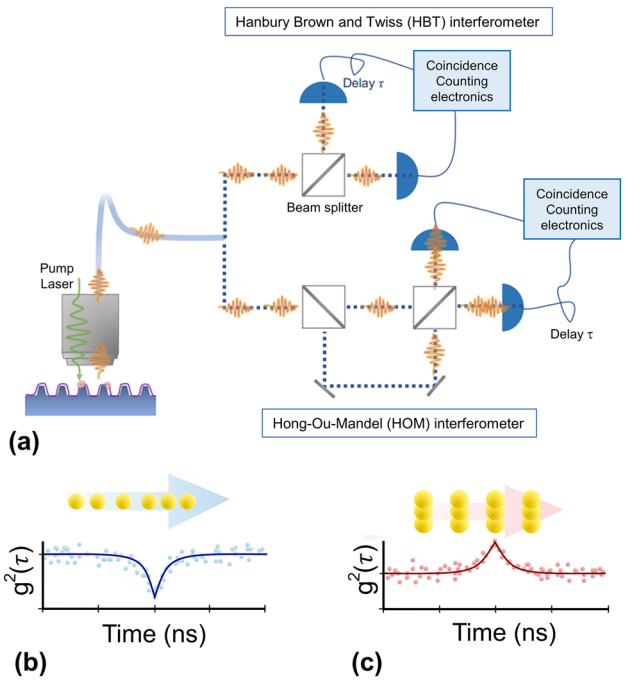

Figure 2. Mechanisms and measurement characteristics of SPE and SR. (a) Schematic representation of an HBT and HOM interferometer. Reproduced with permission.[28] Copyright 2023, American Chemical Society. The second-order autocorrelation measurement results for (b) SPE and (c) SR phenomena.

Photons emitted by an optimal single-photon source exhibit a quantum nature, most notably photon antibunching.[22] This ensures that the time delay between successive photons never falls below a specific minimum value. As shown in [Fig. 2(a)], the experimental verification often involves the Hanbury Brown-Twiss (HBT) interferometer, where a 50:50 beam splitter is used to direct incident photons to two identical optical paths, each ends with an avalanche photodiode.[23] Time-stamped counts are repeatedly measured by the two detectors to generate a second-order autocorrelation histogram of photons detected at different time delays. SPE exhibits a distinct notch around the zero delay, indicative of antibunching behavior, as shown in [Fig. 2(b)].

SPEs can be quantified through several key metrics, including purity, brightness, indistinguishability, and decoherence. Purity is a crucial parameter, demanding a two-level quantum system with a ground state and an excited state that an external perturbation can influence to emit a single photon at a time. The second-order autocorrelation function obtained through the HBT measurements quantifies purity, $g^2(\tau=0)$, which measures the probability of emitting multiple photons simultaneously.[24] For a SPE, a value of $g^2(\tau=0)<0.5$ at zero delay time ($\tau=0$) is required. Brightness in the context of a SPE is directly associated with a higher photon count. This high photon count is achieved when the excited state of the SPE has a short lifetime, indicative of a high radiative decay rate. In optimal scenarios, the SPE should maximally emit in the zero phonon line (ZPL).[25] The ZPL refers to the emission solely attributed to electronic transitions without the involvement of phonons. The Debye–Waller (DW) factor is used to assess the level of electron–phonon coupling, defined as the ratio between the intensity of the ZPL and that of the total emission.[26] A high DW factor is crucial for applications that demand precise and uncontaminated photon emission. The indistinguishability of photons implies minimal spectral diffusion or, in simpler terms, a small spectral linewidth.[27] The spectral linewidth of an SPE should ideally be as low as the Fourier transform of its excited state decay, also known as the emitter's lifetime. The two-photon Hong–Ou–Mandel (HOM) interference [Fig. 2(a)] serves as a powerful tool for detecting the well-defined spatial and temporal modes characteristic of a high-quality SPE.[28] In this measurement, when two indistinguishable single photons are directed into a 50:50 beam splitter, with one in each input port, they invariably exit the beam splitter together in the same output modes. This is a consequence of destructive interference, leading to zero probability for both photons to exit separately. As a result, the coincidence count of exiting photons at zero-time delay is ideally zero, showcasing the precision and reliability of the SPE in generating indistinguishable single photons. Another critical consideration for SPE is achieving minimal decoherence,[29] which requires defect levels to be isolated in energy from the host semiconductors' band edges. Additionally, these defect levels should exhibit real-space localization for effective decoherence mitigation, indicating a smaller defect Bohr radius. This spatial confinement minimizes interactions with the surrounding environment, preventing unwanted influences that could lead to decoherence. In addition to defects, electron–phonon interactions also have a nontrivial contribution to the decoherence.[28]

Superradiance

SR, first described by Dicke in 1954, is a quantum emission phenomenon that has attracted considerable attention in theoretical and experimental research.[5] Dicke first described the phenomenon when researching the radiative decay of N closely confined two-level atoms. When the two-level atoms are noninteracting, their spontaneous emission intensity increases proportionally to the number of two-level atoms or emitters with the radiative decay lifetime of a single atom. However, when these atoms are confined to a volume $V<\lambda^3$, where λ is the emission wavelength of the atoms, they exhibit unique characteristics. The dipole oscillations of the interacting atoms will become phase-locked, forming a giant dipole. This build-up of the individual dipole coupling in the giant dipole results in the emission of an intense and short coherent pulse. The decay rate of the macroscopic dipole increases by a factor of N, resulting in $\Gamma_{SR} \sim N \times \tau_{rad}^{-1}$, where τ_{rad} is the spontaneous radiative decay lifetime of a single atom. The intensity of the coupled pulse becomes $I_{SR} \propto N/T$, where T is the pulse duration and $T \propto N^{-1}$, resulting in $I_{SR} \propto N^2$. These intense and short emission characteristics are hallmarks of Dicke SR.[5,30] Dicke first studied SR in two-level atomic systems. Later on, considerable experimental research has been focused on solid-state systems and molecular aggregates.[13,31,32] These systems also exhibit SR as the properties developed for two-level atoms translate well to other two-level systems of dipoles, usually relying on the relaxation of excitons for emission. This makes exciton delocalization an essential component when studying SR in solid systems.[30,32] Many factors can affect the SR response of a system. For example, radiation decay must be the fastest decay mechanism to achieve SR. Limiting factors of SR decay are primarily inhomogeneous (static) and homogenous (dynamic) dephasing. These dephasing mechanisms can limit the exciton delocalization and coherence of the SR emission, ultimately leading to quenching. Various factors can lead to inhomogeneous dephasing, such as the dipole position and differences in emission energies, while homogeneous dephasing typically arises from exciton-phonon coupling.[30,32–34] Dephasing has been studied in several different systems, with most using low temperatures to mitigate the effects of phonons and highly structured systems to avoid any factors that could limit electron delocalization and coherence.[13,30,32]

Several methods have been used to quantify the SR effect in a system of emitters. These approaches typically leverage the phenomena initially explored by Dicke to demonstrate the presence of SR emission. The most common method involves time-resolved PL (TRPL), which captures emission dynamics. Researchers often compare PL spectra from a low concentration of emitters to that of samples undergoing SR emission, observing an increase in emission intensity and a faster radiative decay rate. This approach has been employed for several decades due to its clear experimental procedures, which closely align with the original characteristics outlined by Dicke.[31,32] Other techniques aim to quantify exciton delocalization and coherence length within a system to evaluate the SR efficacy.[35,36] While these methods predominantly rely on classical emission features, recent studies have increasingly utilized photon-statistics to gauge SR effectiveness. Similar to the study of SPE, SR can also be investigated using the HBT interferometer. However, unlike SPE, which typically exhibits antibunching or $g^2(0) \sim 0$ at the zero-time delay, in SR, bunches of photons are emitted, leading to a $g^2(\tau)$ peak at zero-time delay, a phenomenon known as bunching. This approach to studying SR has been adopted by researchers, who also utilize the bunching peak to assess the strength of SR coherence.[37,38] The so-called bunching behavior in superradiant emission observed through the photon-statistics is schematically shown in Fig. 2(c). SR has been observed in several materials systems, such as epitaxial QDs, quantum wells, and molecular aggregates.[13,34] Recently, PQD has emerged as a new material system to exhibit SPE and SR, with favorable features such as high brightness, high QY, narrow spectral width, etc.

An overview of perovskites

In the past decade, perovskites have captured significant attention for their remarkable performance in solar cells, LEDs, photodetectors, and lasers.[39–41] Recently, perovskites have gained massive interest in quantum optical technologies for exhibiting unique optical and quantum properties such as high QY, brightness, pure SPE, and robust SR. Perovskites generally have the chemical structure of ABX_3 where A is an organic or inorganic cation (e.g., Methylammonium: MA; Formamidinium: FA; Cesium: Cs), B is a metal ion (e.g., Pb, Sn, Bi), and X is a halide anion (e.g., I, Br, Cl).[42] The properties of perovskites can be tuned by adjusting the composition of the A, B, and C components. A schematic of the crystal structure of $CsPbBr_3$ and its transmission electron microscope (TEM) image are shown in [Fig. 3(a) and (b)], respectively.[43] Halide perovskites are generally direct-bandgap semiconductors with bandgaps across the visible spectrum. The bandgap can be tuned by adjusting the composition and size of the QDs [Fig. 3(c)–(e)].[43] The direct bandgap of perovskites lends itself to a very high, near-unity PLQY.[44] The brightness of their emission can also be characterized by sharp PL linewidths, fast radiative lifetimes, and a large oscillator strength.[45,46] The high oscillator strength in lead halide perovskites is attributed to a bright triplet state with orthogonal dipole orientations.[47] The orthogonal dipole orientations can facilitate omnidirectional coupling between nearby QDs, making perovskites a promising material for collective emissions, such as SR.[32] The bright triplet characteristic also explains the fast emission rates of perovskites, which are significantly faster than semiconductor NCs. The coherence times of $CsPbBr_3$ QDs emission have recently been demonstrated to be 80 ps.[48] This combination of fast emission lifetimes and long coherence times makes PQDs extremely promising for SPE and SR applications. Additionally, perovskites have remarkable

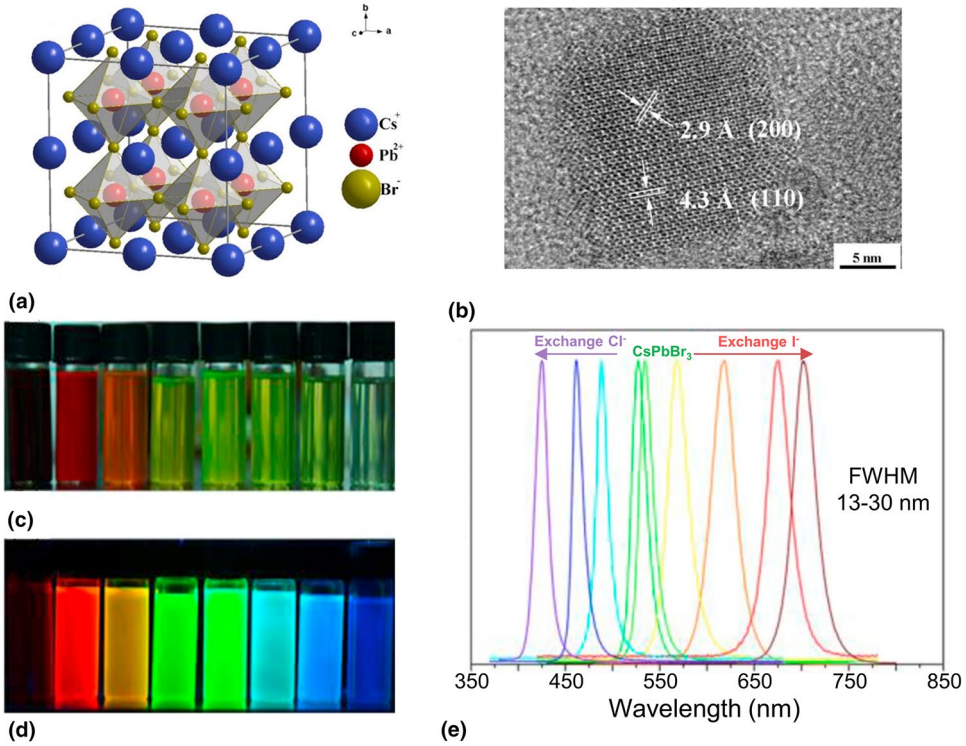

Figure 3. Structure and band gap tunability of lead halide perovskites. (a) Schematic of the cubic ABX_3 (X = Br) perovskite lattice. (b) Corresponding TEM image of the PQD. (c), (d) Optical images of colloidal solutions of different perovskite compositions and sizes under ambient light and a 365 nm UV lamp. (e) PL spectra of halide PQDs. Reproduced with permission.[43] Copyright 2017, Elsevier.

light absorption properties. For example, $MAPbI_3$ has shown an absorption coefficient of up to ~ 10^5 cm^{-1}, which outperforms semiconductors such as Si and GaAs.[49] Most importantly, unlike most semiconductor QDs, the desirable optical properties of perovskites can be observed at room temperature. This operation at room temperature is attributed to the defect tolerance inherent in perovskites. Defect tolerance refers to structural defects, such as vacancies or surface defects, in perovskites residing near the band edges rather than deep within the bandgap. This results in the absence of mid-gap states, which could be detrimental to band gap emission; therefore, PQDs do not require any surface passivation to achieve high PLQYs, unlike conventional semiconductor QDs such as Si, CdSe, or GaAs.[50]

Studies using perovskites for quantum emissions, such as SPE and SR, have used hybrid organic–inorganic lead halide compositions and all inorganic perovskites. The history of perovskite materials traces back to 1893, marked by the synthesis of bulk lead halide perovskite.[51] Almost a century later, Weber et al. synthesized hybrid organic–inorganic perovskite $MAPbX_3$ (X = Cl, Br, I).[52] The desire to combine the exciting optical properties of perovskites with the quantum confinement and processibility benefits of colloidal NCs drove significant research efforts toward synthesizing PQDs. In 2015, Protesescu et al. were the first to demonstrate colloidal $CsPbX_3$ NCs using a facile synthesis technique.[45] $CsPbX_3$ NCs were synthesized by reacting Cs-oleate with a $Pb(II)X_2$ in boiling octadecene solvent at 140–200°C. To solubilize PbX_2 and stabilize the NCs, a mixture of oleylamine and oleic acid was added to the octadecene. The size of the $CsPbX_3$ NCs was found to be easily tunable in the range of 4–15 nm by adjusting the temperature of the reaction. This tunability of size resulted in the wide color range of emission for the NCs, which was found to span the visible region of 410–700 nm. Lead halide perovskites are highly ionic compounds. Thus, they easily form highly crystalline NCs at room temperature and can crystallize into orthorhombic, tetragonal, and cubic polymorphs. Around the same time in 2014, the first colloidal synthesis of organic–inorganic $MAPbBr_3$ was demonstrated by using alkyl ammonium bromide with a medium-sized chain to stabilize crystals in a wide range of solvents.[53] Later, the same group went on to improve the stability of $MAPbBr_3$ by using a quasi-spherical shaped 2-adamantylammonium bromide (ADBr) as a capping ligand. In this work, they also showed a QY of up to 100%.[54] Zhong's group followed this work by using a ligand-assisted reprecipitation (LARP) technique to synthesize $MAPbX_3$ with a tunable bandgap by varying the halide elements.[55]

The facile synthesis methods of PQDs, along with their wide color tunability covering the entire visible spectral region (400–700 nm), make these materials of great interest for a variety of optical applications. The room temperature narrow spectral widths, high PLQY, fast radiative rates, and long coherence times are particularly promising for quantum optical technologies employing SPE and SR.

Single photon emission from perovskite quantum dots

Over the last decade, substantial efforts have been dedicated to advancing the utilization of halide perovskites in the field of quantum optics. However, these emitters faced limitations such as photobleaching and blinking. Subsequently, extensive research has been conducted on SPE from various compositions of perovskites, including all-inorganic cesium lead halide $CsPbX_3$ (X = Cl, Br, I) and hybrid organic–inorganic lead halides perovskites.

This section primarily examines recent advancements in SPE based on both all-inorganic and hybrid perovskite NCs/QDs. Notably, the all-inorganic perovskite, $CsPbX_3$ (X = Cl, Br, I), has received considerable attention for exhibiting pure SPE due to its remarkable stability, brightness, and elevated QY. While few studies have focused on cryogenic temperatures,[48,56] PQDs are renowned for showing SPE at room temperature. The following discussion mainly focuses on their performance at room temperature.[18,57] In 2015, Park and colleagues achieved a noteworthy milestone by demonstrating the first-ever perovskite-based SPE, utilizing all-inorganic $CsPbI_3$ (X = I, Br) QDs.[57] They demonstrated that such QDs acted as excellent quantum emitters with an average $g^2(0)$ value of 0.057. In perovskite systems, antibunching is attributed to the rapid Auger recombination, effectively suppressing the emission from biexcitons and other higher-order multiexcitons. However, their study also showed photodegradation of QDs, particularly in $CsPbBr_3$ and mixed halide perovskites. The PL intensity of the PQDs was found to decrease over time, possibly due to the formation of surface states that induce nonradiative recombination. The size and composition of individual perovskite NCs have been identified as significant factors influencing the purity of SPE. In this context, Zhu et al. investigated the size and composition-dependent quantum confinement effect in the PQD system, exploring its impact on single-photon purity.[18] Single $CsPbX_3$ (X = Br, I) QDs of different compositions and sizes down to 6.6 nm were synthesized. Figure 4(a) displays the PL spectra of all samples, with an inset showing a TEM image of the 6.6 nm $CsPbI_3$ QD.[18] The optical absorption and emission spectra of colloidal $CsPbX_3$ NCs are widely recognized to be tunable across the entire visible spectral region through the adjustment of their composition (ratio of halides in mixed-halide NCs) and particle size, leveraging quantum-size effects. Although $CsPbI_3$ QDs suffer from fast photodegradation and short shelf life, the authors used epoxy-encapsulation to obtain spectrally stable PL, free of photodegradation. The intensity time trace and histogram reflect that the QDs remained in their bright emissive state, with a count rate of around 700 counts per 10 ms, over a long time range [Fig. 4(b)].[18] Finally, they performed second-order autocorrelation measurements for different sizes and compositions of PQDs. However, it has been observed that $CsPbI_3$, with the smallest size of 6.6 nm, showed high single photon purity with $g^2(0) \sim 0.02$ [Fig. 4(c)].[18] Auger recombination between generated excitons was crucial in determining the purity of SPE in such QDs. A recent study by Igarashi et al. further explored the relationship between the SPE behavior and the size (5 to 25 nm) of $CsPbBr_3$ QDs to elucidate potential size thresholds.[58] To do so, the authors synthesized different sizes of PQDs covering the range from firm to no quantum confinement with relative sizes of 0.36 Bohr radius (5 nm) and 1.785 Bohr radii (25 nm) and studied their optical response. The authors also found that a single QD within

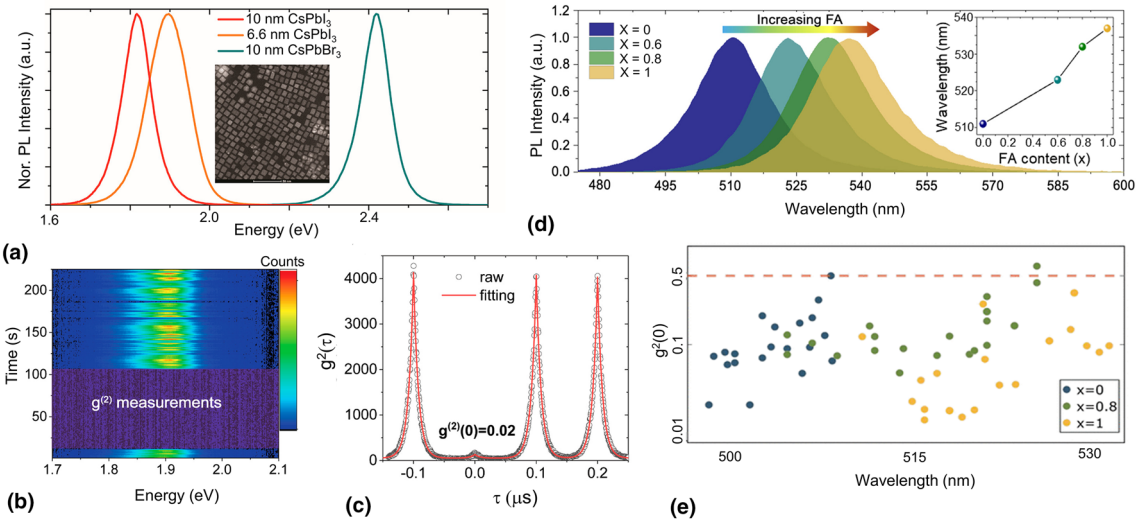

Figure 4. SPE from PQDs. (a) PL spectra from an ensemble of 10 nm $CsPbBr_3$ QDs, 10 nm $CsPbI_3$, and 6.6 nm $CsPbI_3$, all dispersed in toluene. Inset: TEM image of the 6.6 nm $CsPbI_3$ QD. (b) Time series measurements from a single 6.6 nm $CsPbI_3$ QD in an inert atmosphere showcasing the stability of the QDs in the entire illumination period. (c) $g^2(\tau)$ function of a single 6.6 nm $CsPbI_3$ QD. Reproduced with permission.[18] Copyright 2022, American Chemical Society. (d) Tunable fluorescence of the $Cs_{1-x}FA_xPbBr_3$ QDs ensembles ($x = 0$, 0.6, 0.8, and 1). (e) The measured $g^2(0)$ values for the mixed cation PQDs: $CsPbBr_3$ (blue), $Cs_{0.2}FA_{0.8}PbBr_3$ (green), and $FAPbBr_3$ (yellow) as a function of their central emission wavelength. Reproduced with permission.[17] Copyright 2023, American Chemical Society.

the size regime, showing a size-dependent PL spectral shift (quantum-confined QDs smaller than approximately 10 nm), exhibited a high probability of SPE. This probability gradually decreased with an increase in QD size.

In addition to all inorganic ($CsPbX_3$) PQDs, organic–inorganic $FAPbX_3$ QDs have also been reported as efficient single photon emitters.[59] While these QDs frequently experience greater photodegradation and fluorescence intensity intermittency in contrast to all inorganic perovskites, they attract attention for their ability to demonstrate high-purity SPE. Recently, Trinh et al. demonstrated individual $FAPbBr_3$ QD could act as an excellent single-photon source, demonstrating a $g^2(0)$ value of approximately 0.035.[60] Besides all organic and inorganic halide perovskites, mixed cation PQDs have recently gained interest for their enhanced photostability, compositional tunability, and pure SPE. By adjusting the composition of the A-site cations, it is possible to tune the emission wavelength of the QDs over a relatively broad range while maintaining good photostability.[61] This concept has been successfully applied in photovoltaic and light-emitting devices, leading to promising efficiency and brightness.[62,63] In a recent study, D'Amato et al. added FA cation additives into $CsPbI_3$ at different ratios to demonstrate color-tunable SPE.[17] It has been observed that adding FA cation as an additive to QDs can be utilized to finely tune the emission wavelength across more than 30 nm in the visible spectrum, all while retaining excellent single-photon characteristics [Fig. 4(d)].[17]

The full width at half maximums (FWHMs) of the PL spectra of individual $Cs_{1-x}FA_xPbBr_3$ were found to be 69.16 meV (~14 nm) to 79.78 meV (~16 nm) for x = 0, from 69.65 meV (~14.5 nm) to 82.45 meV (~18 nm) for $x = 0.8$, and from 78.19 meV (~17.6 nm) to 88.24 meV (~19 nm) for x = 1. However, a relatively higher level of photo instability was observed in the organic–inorganic $FAPbBr_3$ perovskites compared to the all-inorganic $CsPbBr_3$, as well-documented in the literature.[64] Finally, the authors performed second-order autocorrelation measurements to study the purity of the single photon emitters. As shown in [Fig. 4(e)], the majority of $CsPbBr_3$ (56%), $Cs_{0.2}FA_{0.8}PbBr_3$ (55%), and $FAPbBr_3$ (75%) QDs have $g^2(0)$ values less than the 0.1 demonstrating high purity of the SPE.[17] It has also been observed that emitters with relatively smaller emission wavelengths exhibit improved purity compared to those with the same composition. This improvement is attributed to the higher quantum confinement effect in the smaller QDs. In another study, Hsu et al. employed an unconventional spray synthesis technique to produce $CsPbI_3$ PQDs.[65] They not only observed a higher brightness of 9×10^6 counts/s and a high purity ($g^2(0) = 0.021$) but also demonstrated the PQDs' high stability without any photobleaching for up to 24 h.

One of the significant limitations of PQDs-based quantum emitters is blinking, the random fluctuation of the emitted intensity of a QD. Such a behavior has been reported in quantum emitters, including single molecules, Si NCs, and CdSe/CdS colloidal QDs.[66,67] Usually, the fluorescence blinking is attributed to the trapping of charge carriers. In the conventional blinking model [Fig. 5(a)], ON and OFF periods correspond respectively to a neutral NC and a charged NC. Photo-assisted charging/discharging induces random switching between these two states. The dynamics of the bright state are primarily governed by the radiative recombination of the neutral exciton, X^0. Conversely, for a charged exciton (trion) X^-, three-particle Auger recombination initiates a rapid, non-radiative channel, resulting in a diminished PLQY.[68] In particular, it has been

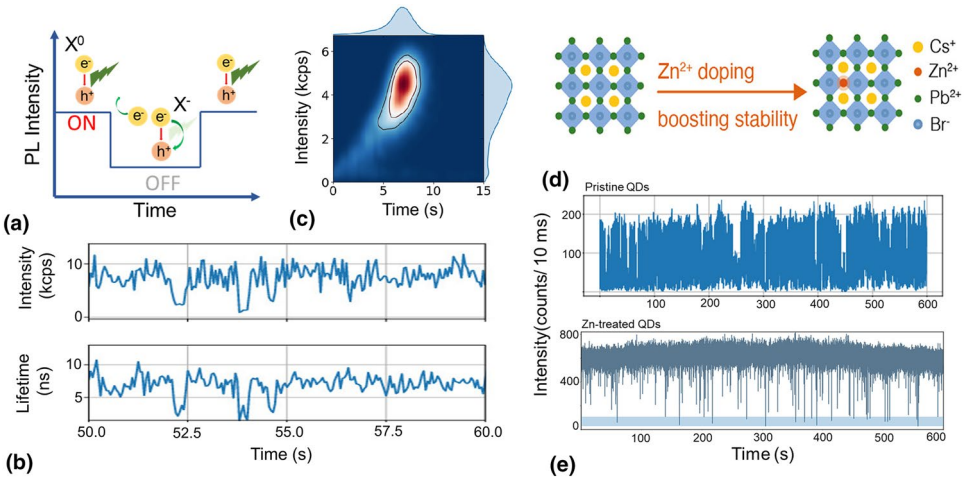

Figure 5. Blinking of PQDs. (a) Schematic representation of a conventional (Type A) blinking model, ON and OFF periods correspond to a neutral NC (X^0) and a charged NC (X^-), respectively. (b) Time trace plot for PL intensity (upper graph) and corresponding lifetime (lower graph) of a single QD. (c) Fluorescence lifetime-intensity distribution (FLID) images of a single emitter.[69] Copyright 2020, American Chemical Society. (d) Schematic representation of Zn^{2+} ion doping at the Pb-site of $CsPbBr_3$ to enhance its stability. (e) PL intensity time trace measurements for pristine (upper graph) and Zn-treated PQDs (lower graph), showing reduced blinking in treated QDs. Reproduced with permission.[76] Copyright 2023, American Chemical Society.

observed that blinking occurs through two distinct mechanisms, denoted as type A and type B. Type A blinking is generated due to the transition between neutral (ON) and charged excitonic (OFF) states, and the low fluorescence state is caused by recombination due to the Auger effect. Type A blinking is prevalent in PQDs, and most of the quantum emitters mentioned above exhibit this kind of blinking. On the other hand, in type B blinking, the charge can recombine non-radiatively, and the blinking is due to fluctuations in the trapping rate. A well-established method to experimentally distinguish between type A and type B blinking is to examine the dependence of spontaneous emission lifetime on the emission intensity. In type A blinking, the lifetime is expected to depend on the emission intensity, while in type B, there is no such dependence.[68] When the blinking time is too short compared to the chosen binning of the time-trace curve, it becomes challenging to fully distinguish between ON and OFF states. In such cases, it is more appropriate to describe the behavior of the emitter in terms of flickering. For example, a clear blinking in the case of $CsPbBr_3$ nanocubes could be observed through an intensity time-trace experiment, where the emitted intensity is plotted as a function of time, as shown in [Fig. 5(b)].[69] The mean lifetime versus time is shown in the lower panel of [Fig. 5(b)], revealing a clear correlation between the lifetime and emission intensity. This correlation indicates the presence of Type A blinking for these emitters. Another convenient tool for analyzing correlations between fluorescence intensities and lifetimes is a fluorescence lifetime–intensity distribution (FLID) representation. This representation shows the probability of occupying a given state in the two-dimensional lifetime–intensity space. An example of type A blinking in FLID is illustrated in [Fig. 5(c)].[69]

In this context, considerable efforts have been employed to suppress the blinking and to develop highly stable perovskite systems with high PLQY and strong luminescence emission. Various strategies have been used, including ligand passivation,[70] surrounding shell growth,[71] and embedding NCs in a protective matrix to shield them from moisture exposure.[72] Another widely adopted approach involves B-site metal doping, where bivalent or heterovalent metal ions, such as Mn^{2+}, Ni^{2+}, Cu^{2+}, Ba^{2+}, Ce^{2+}, Sn^{2+}, and rare earth ions, are incorporated to stabilize the crystalline phases of perovskites and finely tune their optical properties.[73] Theoretical predictions suggest that doping with smaller metal ions enhances the tolerance factor, thereby improving the stability of the lattice structure. Additionally, doping smaller foreign metal ions induces lattice contraction, leading to shorter metal ion–X bonds, improved short-range order, and reduced halide vacancies in the doped perovskites.[74,75] The concept of doping has proven highly effective in the development of robust quantum emitters as well. For example, D'Amanto et al. recently demonstrated that doping Zn^{2+} ions at the Pb-sites improved the stability of diluted $CsPbBr_3$ QDs under illumination [Fig. 5(d)].[76] The stability of the PQDs was further evaluated for different dilutions at ambient conditions, which showed enhanced stability in the case of Zn doping. Further investigations indicated a significant reduction in blinking behavior for the Zn-treated $CsPbBr_3$ QDs [Fig. 5(e)].[76] Photon antibunching measurements were also carried out, demonstrating an increase in single-photon purity after being treated with Zn. Until now, numerous efforts have been made to mitigate blinking and degradation in PQDs through various studies.[77,78] However, their potential as stable and bright SPEs awaits further explorations.

Superradiance from perovskite quantum dots

Successful demonstration of coherence in quantum optical systems has motivated significant research efforts over the past decade. As outlined in a previous section, SR is a macroscopic coherent state, which has been demonstrated in several systems, such as molecular aggregates,[12] nitrogen-vacancy centers,[79] and epitaxially grown QDs.[31] Observing SR is difficult due to inherent inhomogeneities and fast dephasing processes in solid materials.[30,32] Recently, lead halide PQDs have come forth as potential candidates for SR. This is due to their robust optical properties, such as near unity PLQYs, long coherence time, extended exciton delocalization, and unique omnidirectional coupling capabilities, as outlined previously.

In a recent study by Blach et al., SR was demonstrated in $CsPbBr_3$ QDs arranged in superlattices (SL) at a low temperature (11 K).[35] In the past, coupled emitters in SLs have been employed for collective effects in semiconductor QDs.[80] Closely packed QD SLs with high ordering can facilitate coherent quantum emission due to the coupling between individual emitters. Another advantage of PQD SLs is the ease of assembling the individual QDs into the ordered SL. The cubic PQDs tend to be tightly self-assembled on a substrate into regular geometric configurations.[81] A slow and controlled vacuum evaporation step then enables the QDs of similar size to aggregate and align into SLs. The size selectivity of the self-assembly method results in long-range and highly ordered SLs with minimal defects.[35] Blach et al. used fast Fourier transforms (FFTs) of high-angle annular dark-field imaging scanning transmission electron microscopy (HAADF-STEM) images to confirm the ordering of their SLs. Figure 6(a) shows the HAADF-STEM image of a $CsPbBr_3$ SL with the FFT in the inset.[35] Based on the positions of reflections from FFT images; the researchers determined a length of 9 nm QD with 3 nm spacings due to capping ligands for their SL. The spacing between QDs was used to calculate the nearest neighbor dipole–dipole coupling. The dipole–dipole coupling is proportional to the SL-induced energy shift.[82] This was confirmed by measuring temperature-dependent PL spectra of the SL. The authors found the dipole–dipole coupling to be ~16 meV, the same order of magnitude as the PL peak shift at 11 K. Further evidence of SR is observed by measuring the temperature-dependent PL of the SL, as shown in Fig. 6(b).[35] The SLs have a red-shifted and narrower PL emission at 11 K compared to isolated QDs, which the researchers attributed to collective excitonic states. To give more proof of SR, the researchers performed low-temperature

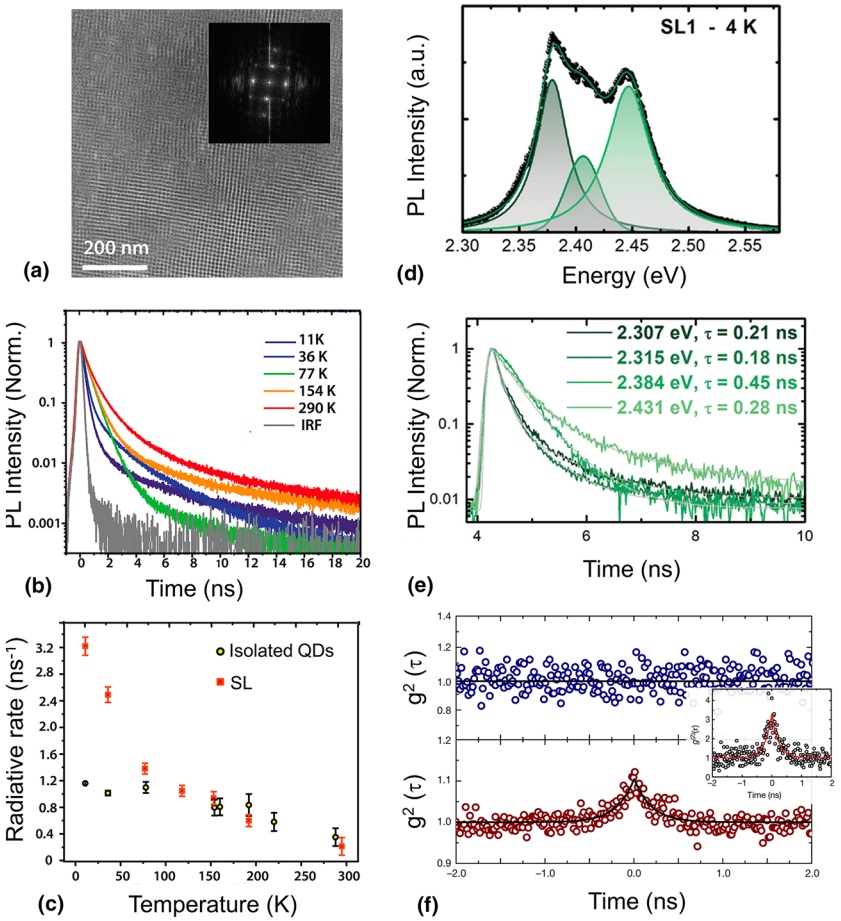

Figure 6. Superradiant emission from perovskite SLs. (a) High-resolution HAADF-STEM image of a $CsPbBr_3$ SL fabricated through self-assembly of QDs. Inset: FFT image to exemplify high ordering of the SL. (b) Temperature-dependent TRPL of an SL showing a fast lifetime of superradiant emission. (c) Temperature-dependent calculated radiative rates of isolated QDs in a PMMA matrix (black data points) and an SL (red data points). Reproduced with permission.[35] Copyright 2022, American Chemical Society. (d) PL spectra of a $CsPbBr_3$ perovskite SL at 4 K reveal high and low energy peaks attributed to isolated and coupled QDs in the SL, respectively. (e) TRPL traces at 4 K with varying emission energies reveal that the low energy emission attributed to SR has a shortened lifetime. Reproduced with permission.[83] Copyright 2023, Wiley–VCH. (f) The second-order autocorrelation function, $g^2(\tau)$, taken for a $CsPbBr_3$ PQD SL at 6 K. The second-order autocorrelation function, $g^2(\tau)$ observed at the high energy emission is shown above in blue, and the $g^2(\tau)$ for the redshifted lower energy emission is shown below in red. The emission associated with the SL shows clear bunching behavior characteristic of correlated emission. Inset: An example of superbunching with $g^2(0) > 2$ from a single SL. Reproduced with permission.[85] Copyright 2015, Nature.

TRPL measurements to compare the radiative rates of an SL to that of an isolated QD [Fig. 6(c)].[35] The radiative rates were estimated by comparing the PLQY to the experimental PL decay time and were found to be approximately two times higher than the isolated QDs at 11 K.

Recently, Adl et al. also showed evidence for SR in $CsPbBr_3$ and $CsPbI_3$ SLs.[83] Using a similar approach, they compared low-temperature (4 K) PL spectra of SLs and isolated QDs. However, instead of seeing a single PL peak for the SLs described in previous work, high-energy and low-energy peaks are visible, as shown in [Fig. 6(d)].[35,83] The appearance of two peaks for PQD SLs has been observed before by Zhou et al., where a second narrower and red-shifted peak arises due to the superposition of the single QD's excitonic wavefunctions in the SL.[79] The dynamics of the low and high energy peaks from SLs were further investigated by looking at TRPL at varying emission wavelengths using a confocal PL and TRPL setup at 4 K [Fig. 6(e)].[83] It was observed that the low energy peaks attributed to SR had much faster emission decay than those at higher energies. Additionally, the authors found that the high energy peaks attributed to emission from isolated QDs in the SL behave similarly to emission from isolated QDs in film on a separate sample. PQDs have also shown evidence of superfluorescence (SF), an enhanced emission state similar to SR but excited by quantum many-body effects.[32,79,84] In 2018, Raino et al. achieved SF from lead halide PQD SLs at 6 K.[85] The authors performed second-order autocorrelation measurements to prove the SR effect in their system, as illustrated in [Fig. 6(f)].[85] It could be distinctly observed that the SF band exhibits a $g^2(0)$ value exceeding 1, in contrast to the band

associated with uncoupled QDs, which displays a consistent flat line. Superbunching with $g^2(0) > 2$ was also observed for a single SL, as shown in the inset in [Fig. 6(f)]. A very recent work in 2024 by Zhu et al. has taken a different approach to achieving SR in PQDs.[86] In this study, the researchers took advantage of the excitation delocalization of large QDs in the weak quantum confinement regime due to the size being much larger than the Bohr diameter. Lifetimes for various sizes of PQDs were measured, revealing that at 4 K, the large QDs (23 nm) exhibited enhanced radiative lifetimes attributed to single-photon superradiance (SPS).

As mentioned earlier, much of the SR phenomenon in solid materials depends on the relaxation of excitons. This makes exciton delocalization an essential factor when considering the possibility of SR in a potential emitter. While these materials make promising candidates for superradiant emission, researchers have found similar limiting factors for other solid emitters. As discussed in the earlier section, homogeneous or dynamic, as well as inhomogeneous or static dephasing, are the main factors leading to the suppression of superradiant coherent emission. While this dephasing challenge persists across all superradiant solid systems, researchers have particularly focused on addressing this issue for PQDs.[35,81,84,87,88] It can be especially difficult to experimentally explore the effects of spatial and inhomogeneous dephasing due to the rigorous specifications that can be required in systems. Computational simulations and models, on the other hand, have been employed to study dephasing.[81,87] Nguyen et al. used the tight-binding Hamiltonian to model lead halide perovskite NCs forming 2D and 3D SLs to study the effects of static disorder and how they might be optimized for SR.[81] The researchers also tuned several factors, such as the size and separation of nanoparticles, spatial disorder, etc. They discovered that perovskites with nearly identical characteristics exhibited a greater radiative enhancement when compared to highly ordered SLs. They also found that cubic SL arrays with more emitters experienced higher exciton delocalization and enhancement of SR than SLs with fewer emitters.[81] Mattiotti et al. simulated similar cubic structures for the same size of emitters and found that tighter packing of the PQDs led to enhanced superradiant emission.[87] Through these simulations, experimentalists can make highly coupled and coherent SLs by bypassing the limitations of static dephasing, which has continuously limited their use for application processes.[30,32,81,87,89]

Other studies have focused on the dynamic dephasing of the coherent superradiant emission in solid systems. A primary focal point of interest lies in thermal dephasing.[34,35,83,87] Superradiant emissions primarily operate within cryogenic temperatures, presenting a barrier to their practical implementation.[32] However, there has been some work to have coherently coupled emitters remain in phase at room temperature. Recent work on SR in J-aggregates has shown a short radiative lifetime of 29 ps under these conditions.[90] However, homogeneous broadening still limits the exciton delocalization for perovskites at room temperature.[84] Blach et al. employed TRPL to quantify exciton delocalization at different temperatures in cubic SLs of colloidal $CsPbBr_3$, as described earlier in this Section.[35] TRPL carried out between 11 and 220 K revealed an increased radiative rate at temperatures lower than 100 K, as seen in [Fig. 6(c)].[35] At lower temperatures, phonon scattering, which usually localizes excitons, is suppressed, increasing their range and ability to enter a cooperative emissive state.[34,83] They also extracted the phonon scattering strength after fitting PL linewidth obtained from the temperature-dependent PL data, which revealed that coupling of optical phonons dominated the temperature-dependent profile over the acoustic ones. Researchers such as Biliroglu et al. developed inventive ways to overcome the obstacles associated with coherent quantum emissions at room temperature.[84] The group employed a technique that they termed a quantum analog mechanism for vibrational isolation (QAVI) to demonstrate room temperature SF in a quasi 2D phenethylammonium cesium lead bromide (PEA: $CsPbBr_3$) perovskite thin film. These films went through a phase transition in which polarons were formed that intrinsically acted as a spring isolator to phonon perturbations and extended the electronic coherence length in the emission. The coherence of hybrid perovskites has been shown to be less affected by thermal noise than all inorganic perovskites.[91] These promising findings from several studies on hybrid perovskites indicate an exciting new opportunity for utilizing hybrid PQDs in room temperature superradiant phenomena. In this direction, Zhu et al. suggested a theory where the freely rotating organic cation in hybrid perovskites can screen hot carriers from scattering with longitudinal optical phonons.[92] In contrast, a study by Conibeer et al. found that the isolation of carrier-phonon cooling in hybrid perovskite thin films was due to an up-conversion of the acoustic phonon modes, which leads to a recycling of energy and re-excitation of carriers, thus elongating carrier lifetimes.[91] This was shown to occur due to the presence of low-energy optical phonon modes from the organic cation. Regardless of the origin of such thermal isolation, this phenomenon has profound implications for possibly demonstrating room temperature SR in PQDs.

Conclusion & outlook

The quest for an optimal quantum emitter for applications has propelled numerous researchers in the past decades to explore various materials. Indeed, several candidate materials, such as atom-like defects in diamonds, hBN, 2D TMDs, fluorescent dye molecules, and semiconductor QDs, have exhibited single photon behavior. On the other hand, SR has been shown in epitaxial QDs, quantum wells, and molecular aggregates. However, the exploration of these materials has been hindered by several challenges, including low emitter density, reduced QY, uncontrollable defects, conventional fabrication processes, and the necessity for low-temperature operability. However, the diverse compositions of perovskite NCs and QDs have recently generated considerable interest in advancing quantum optical technologies driven by their unique properties. These

properties are attributed to several factors, including their ease of synthesis, remarkable brightness, tunable fluorescence, and exceptionally high QY. Often, PQDs exhibit high-purity SPE and robust SR, making them unique candidates for quantum emission applications.

Despite having several unique properties, PQDs still face several challenges. Namely, the stability of these materials is a major roadblock. The decomposition of PQDs is accelerated by ambient conditions such as moisture, oxygen, heat, and light. Additionally, all lead halide perovskite NCs suffer from instability in polar solvents and ambient atmosphere. Since stability is one of the key parameters of any technology, more studies should be conducted to develop a stable and robust PQD-based quantum emitter. Although, several strategies have been employed so far to increase the stability of the PQDs. Still, significant room remains for enhancing the stability of PQDs, a factor crucial to SPE and SR. Exploring the impact of strain, electrical, and magnetic fields is imperative to comprehensively understand quantum emission behavior. While PQDs are renowned for their ability to produce highly pure single photons, the journey toward on-chip integration of single photons still requires substantial progress.

Despite the defect tolerance of perovskites contributing to impressive SPE performance at room temperature, studies on SR in PQDs have primarily been limited to low temperatures.[35,79,83,87] Thermal dephasing due to exciton-phonon coupling leads to a broadening of the spectral linewidth, limiting the coherent coupling of microscopic states. It has been proposed, however, that hybrid organic–inorganic perovskites may be protected from thermal dephasing due to large polarons that isolate electronic excitations. The use of hybrid perovskites for quantum emission is still open for many investigations and might be an exciting topic for room temperature SR. More studies on modeling and simulation are needed to create a realistic picture to better understand the dephasing process in such systems. Additionally, most of the research works presented so far show evidence of SR from PQD-based SLs by analyzing PL spectra and TRPL. One experiment lacking so far is the demonstration of photon statistics by using second-order autocorrelation measurement employing HBT interferometer.

With the rapid development of artificial intelligence (AI), machine learning (ML), including large language models (LLMs), and automated robotics could also play a pivotal role in driving significant advancements in this field.[93,94] The stability and purity of these PQDs are essential in determining their efficacy in quantum technologies. In this regard, ML can accelerate the discovery of stable PQDs through compositional screening and learning the trends between compositional ratios and responses to environmental stressors.[95,96] With the increasing number of studies on PQDs, LLMs could be invaluable for gaining detailed insights into this class of materials. LLMs can analyze vast amounts of scientific literatures, experimental data, and research findings, helping researchers identify key trends, emerging patterns, and novel hypotheses more efficiently than traditional methods.[97] Automated synthesis and characterization can also play a crucial role in the industrialization of PQDs in the field of quantum technologies. By using advanced robotics and AI-driven systems, these processes can be scaled up to meet industrial demands while maintaining high precision and consistency. Automated synthesis could ensure that the production of PQDs is both rapid and reproducible, reducing variability and enhancing quality control.[98] Similarly, automated characterization allows for real-time monitoring and analysis of PQD properties and characteristics to quickly identify optimal synthesis parameters and ensure that the produced materials meet the desired specifications.[99]

Despite facing numerous obstacles, there is a growing interest in advancing perovskite-based quantum emitters. With ongoing advancements in synthesizing advanced PQDs and device fabrication techniques, it is anticipated that PQD-based quantum emitters could serve as a robust material platform for future quantum optical applications.

Acknowledgments

We acknowledge the support from National Science Foundation, Welch Foundation, and the Air Force Office of Scientific Research.

Author contributions

A.C. and S.H. conceived the idea. All authors contributed to the writing of the manuscript. S.H. supervised the project.

Funding

This work was supported by the National Science Foundation (ECCS-2230400, ECCS-1943895, and ECCS-2246564), Welch Foundation (C-2144), and the Air Force Office of Scientific Research (FA9550-22-1-0408).

Declarations

Conflict of interest

On behalf of all authors, the corresponding author states that there is no conflict of interest.

References

1. M. Bozzio, M. Vyvlecka, M. Cosacchi, C. Nawrath, T. Seidelmann, J.C. Loredo, S.L. Portalupi, V.M. Axt, P. Michler, P. Walther, Npj Quantum Inf. **8**, 104 (2022)
2. M. Pompili, S.L.N. Hermans, S. Baier, H.K.C. Beukers, P.C. Humphreys, R.N. Schouten, R.F.L. Vermeulen, M.J. Tiggelman, L. Dos Santos Martins, B. Dirkse, S. Wehner, R. Hanson, Science **372**, 259–264 (2021)
3. D.-W. Wang, M.O. Scully, Phys. Rev. Lett. **113**, 083601 (2014)
4. Z. Zhang, L.M. Duan, New J. Phys. **16**, 103037 (2014)
5. R.H. Dicke, Phys. Rev. **93**, 99–110 (1954)
6. J. Martín-Sánchez, G. Muñoz-Matutano, J. Herranz, J. Canet-Ferrer, B. Alén, Y. González, P. Alonso-González, D. Fuster, L. González, J. Martínez-Pastor, F. Briones, ACS Nano **3**, 1513–1517 (2009)
7. J. Hours, S. Varoutsis, M. Gallart, J. Bloch, I. Robert-Philip, A. Cavanna, I. Abram, F. Laruelle, J.M. Gérard, Appl. Phys. Lett. **82**, 2206–2208 (2003)

8. D. Dalacu, P.J. Poole, R.L. Williams, Nanotechnology **30**, 232001 (2019)
9. L. Gan, D. Zhang, R. Zhang, Q. Zhang, H. Sun, Y. Li, C.-Z. Ning, ACS Nano **16**, 14254–14261 (2022)
10. W. Wang, L.O. Jones, J.-S. Chen, G.C. Schatz, X. Ma, ACS Nano **16**, 21240–21247 (2022)
11. M. Arita, F. Le Roux, M.J. Holmes, S. Kako, Y. Arakawa, Nano Lett. **17**, 2902–2907 (2017)
12. F.C. Spano, S. Mukamel, J. Chem. Phys. **91**, 683–700 (1989)
13. C. Bradac, M.T. Johnsson, M.V. Breugel, B.Q. Baragiola, R. Martin, M.L. Juan, G.K. Brennen, T. Volz, Nat. Commun. **8**, 1205 (2017)
14. W. Zhang, E.R. Brown, A. Mingardi, R.P. Mirin, N. Jahed, D. Saeedkia, Appl. Sci. **9**, 3014 (2019)
15. J. Shamsi, A.S. Urban, M. Imran, L. De Trizio, L. Manna, Chem. Rev. **119**, 3296–3348 (2019)
16. A. Das, A. Ghorai, K. Saha, A. Chatterjee, U. Jeong, J. Mater. Chem. A. **11**, 6796–6813 (2023)
17. M. D'Amato, Q.Y. Tan, Q. Glorieux, A. Bramati, C. Soci, ACS Photonics **10**, 197–205 (2023)
18. C. Zhu, M. Marczak, L. Feld, S.C. Boehme, C. Bernasconi, A. Moskalenko, I. Cherniukh, D. Dirin, M.I. Bodnarchuk, M.V. Kovalenko, G. Rainò, Nano Lett. **22**, 3751–3760 (2022)
19. A.M. Fox, *Quantum Optics: An Introduction* (Oxford University Press, Oxford, 2006)
20. C. Couteau, S. Barz, T. Durt, T. Gerrits, J. Huwer, R. Prevedel, J. Rarity, A. Shields, G. Weihs, Nat. Rev. Phys. **5**, 326–338 (2023)
21. E. Meyer-Scott, C. Silberhorn, A. Migdall, Rev. Sci. Instrum. **91**, 041101 (2020)
22. H.J. Kimble, M. Dagenais, L. Mandel, Phys. Rev. Lett. **39**, 691–695 (1977)
23. R.H. Brown, R.Q. Twiss, Lond. Edinb. Dublin Philos. Mag. J. Sci. **45**, 663–682 (1954)
24. R.H. Brown, R.Q. Twiss, Nature **177**, 27–29 (1956)
25. J. Wolters, A.W. Schell, G. Kewes, N. Nüsse, M. Schoengen, H. Döscher, T. Hannappel, B. Löchel, M. Barth, O. Benson, Appl. Phys. Lett. **97**, 141108 (2010)
26. E. Neu, D. Steinmetz, J. Riedrich-Möller, S. Gsell, M. Fischer, M. Schreck, C. Becher, New J. Phys. **13**, 025012 (2011)
27. C. Santori, D. Fattal, J. Vučković, G.S. Solomon, Y. Yamamoto, Nature **419**, 594–597 (2023)
28. S. Gupta, W. Wu, S. Huang, B.I. Yakobson, J. Phys. Chem. Lett. **14**, 3274–3284 (2023)
29. V. D'Auria, N. Lee, T. Amri, C. Fabre, J. Laurat, Phys. Rev. Lett. **107**, 050504 (2011)
30. K. Cong, Q. Zhang, Y. Wang, G.T. Noe, A. Belyanin, J. Kono, JOSA B. **33**, C80–C101 (2016)
31. M. Scheibner, T. Schmidt, L. Worschech, A. Forchel, G. Bacher, T. Passow, D. Hommel, Nat. Phys. **3**, 106–110 (2007)
32. G. Rainò, H. Utzat, M.G. Bawendi, M.V. Kovalenko, MRS Bull. **45**, 841–848 (2020)
33. S. Lyagushyn, A. Sokolovsky, Low Temp. Phys. **50**, 103–109 (2024)
34. D.H. Arias, K.W. Stone, S.M. Vlaming, B.J. Walker, M.G. Bawendi, R.J. Silbey, V. Bulović, K.A. Nelson, J. Phys. Chem. B **117**, 4553–4559 (2013)
35. D.D. Blach, V.A. Lumsargis, D.E. Clark, C. Chuang, K. Wang, L. Dou, R.D. Schaller, J. Cao, C.W. Li, L. Huang, Nano Lett. **22**, 7811–7818 (2022)
36. A.D. Bailey, A.P. Deshmukh, N.C. Bradbury, M. Pengshung, T.L. Atallah, J.A. Williams, U. Barotov, D. Neuhauser, E.M. Sletten, J.R. Caram, Nanoscale **15**, 3841–3849 (2023)
37. C. Hettich, C. Schmitt, J. Zitzmann, S. Kühn, I. Gerhardt, V. Sandoghdar, Science **298**, 385–389 (2002)
38. J.Q. Grim, A.S. Bracker, M. Zalalutdinov, S.G. Carter, A.C. Kozen, M. Kim, C.S. Kim, J.T. Mlack, M. Yakes, B. Lee, D. Gammon, Nat. Mater. **18**, 963–969 (2019)
39. Y. Zhao, K. Zhu, Chem. Soc. Rev. **45**, 655–689 (2016)
40. H. Wang, D.H. Kim, Chem. Soc. Rev. **46**, 5204–5236 (2017)
41. W. Zhang, G.E. Eperon, H.J. Snaith, Nat. Energy **1**, 16048 (2016)
42. Q. Ou, X. Bao, Y. Zhang, H. Shao, G. Xing, X. Li, L. Shao, Q. Bao, Nano Mater. Sci. **1**, 268–287 (2019)
43. S. Liu, G. Chen, Y. Huang, S. Lin, Y. Zhang, M. He, W. Xiang, X. Liang, J. Alloys Compd. **724**, 889–896 (2017)
44. I.L. Braly, D.W. deQuilettes, L.M. Pazos-Outón, S. Burke, M.E. Ziffer, D.S. Ginger, H.W. Hillhouse, Nat. Photonics **12**, 355–361 (2018)
45. L. Protesescu, S. Yakunin, M.I. Bodnarchuk, F. Krieg, R. Caputo, C.H. Hendon, R.X. Yang, A. Walsh, M.V. Kovalenko, Nano Lett. **15**, 3692–3696 (2015)
46. S. Bai, Z. Yuan, F. Gao, J. Mater. Chem. C **4**, 3898–3904 (2016)
47. M.A. Becker, R. Vaxenburg, G. Nedelcu, P.C. Sercel, A. Shabaev, M.J. Mehl, J.G. Michopoulos, S.G. Lambrakos, N. Bernstein, J.L. Lyons, T. Stöferle, R.F. Mahrt, M.V. Kovalenko, D.J. Norris, G. Rainò, A.L. Efros, Nature **553**, 189–193 (2018)
48. H. Utzat, W. Sun, A.E.K. Kaplan, F. Krieg, M. Ginterseder, B. Spokoyny, N.D. Klein, K.E. Shulenberger, C.F. Perkinson, M.V. Kovalenko, M.G. Bawendi, Science **363**, 1068–1072 (2019)
49. T.M. Brenner, D.A. Egger, L. Kronik, G. Hodes, D. Cahen, Nat. Rev. Mater. **1**, 1–16 (2016)
50. H. Huang, M.I. Bodnarchuk, S.V. Kershaw, M.V. Kovalenko, A.L. Rogach, ACS Energy Lett. **2**, 2071–2083 (2017)
51. H.L. Wells, Z. Für Anorg. Chem. **3**, 195–210 (1893)
52. D. Weber, Z. Für Naturforschung B. **33**, 1443–1445 (1978)
53. L.C. Schmidt, A. Pertegás, S. González-Carrero, O. Malinkiewicz, S. Agouram, G. Mínguez Espallargas, H.J. Bolink, R.E. Galian, J. Pérez-Prieto, J. Am. Chem. Soc. **136**, 850–853 (2014)
54. S. Gonzalez-Carrero, L. Francés-Soriano, M. González-Béjar, S. Agouram, R.E. Galian, J. Pérez-Prieto, Small **12**, 5245–5250 (2016)
55. F. Zhang, H. Zhong, C. Chen, X. Wu, X. Hu, H. Huang, J. Han, B. Zou, Y. Dong, ACS Nano **9**, 4533–4542 (2015)
56. F. Hu, H. Zhang, C. Sun, C. Yin, B. Lv, C. Zhang, W.W. Yu, X. Wang, Y. Zhang, M. Xiao, ACS Nano **9**, 12410–12416 (2015)
57. Y.-S. Park, S. Guo, N.S. Makarov, V.I. Klimov, ACS Nano **9**, 10386–10393 (2015)
58. H. Igarashi, M. Yamauchi, S. Masuo, J. Phys. Chem. Lett. **14**, 2441–2447 (2023)
59. J. Liu, F. Hu, Y. Zhou, C. Zhang, X. Wang, M. Xiao, J. Lumin. **221**, 117032 (2020)
60. C.T. Trinh, D.N. Minh, K.J. Ahn, Y. Kang, K.-G. Lee, ACS Photonics **5**, 4937–4943 (2018)
61. D. Chen, X. Chen, Z. Wan, G. Fang, ACS Appl. Mater. Interfaces **9**, 20671–20678 (2017)
62. A. Hazarika, Q. Zhao, E.A. Gaulding, J.A. Christians, B. Dou, A.R. Marshall, T. Moot, J.J. Berry, J.C. Johnson, J.M. Luther, ACS Nano **12**, 10327–10337 (2018)
63. Y.-W. Zhang, G. Wu, H. Dang, K. Ma, S. Chen, Ind. Eng. Chem. Res. **56**, 10053–10059 (2017)
64. Z. Ahmad, M.A. Najeeb, R.A. Shakoor, A. Alashraf, S.A. Al-Muhtaseb, A. Soliman, M.K. Nazeeruddin, Sci. Rep. **7**, 15406 (2017)
65. B.-W. Hsu, Y.-T. Chuang, C.-Y. Cheng, C.-Y. Chen, Y.-J. Chen, A. Brumberg, L. Yang, Y.-S. Huang, R.D. Schaller, L.-J. Chen, C.-S. Chuu, H.-W. Lin, ACS Nano **15**, 11358–11368 (2021)
66. M. Nirmal, B.O. Dabbousi, M.G. Bawendi, J.J. Macklin, J.K. Trautman, T.D. Harris, L.E. Brus, Nature **383**, 802–804 (1996)
67. B. Mahler, P. Spinicelli, S. Buil, X. Quelin, J.-P. Hermier, B. Dubertret, Nat. Mater. **7**, 659–664 (2008)
68. C. Galland, Y. Ghosh, A. Steinbrück, M. Sykora, J.A. Hollingsworth, V.I. Klimov, H. Htoon, Nature **479**, 203–207 (2011)
69. S. Pierini, M. D'Amato, M. Goyal, Q. Glorieux, E. Giacobino, E. Lhuillier, C. Couteau, A. Bramati, ACS Photonics **7**, 2265–2272 (2020)
70. B. Zhang, L. Goldoni, C. Lambruschini, L. Moni, M. Imran, A. Pianetti, V. Pinchetti, S. Brovelli, L. De Trizio, L. Manna, Nano Lett. **20**, 8847–8853 (2020)
71. M.N. An, S. Park, R. Brescia, M. Lutfullin, L. Sinatra, O.M. Bakr, L. De Trizio, L. Manna, ACS Energy Lett. **6**, 900–907 (2021)
72. S.N. Raja, Y. Bekenstein, M.A. Koc, S. Fischer, D. Zhang, L. Lin, R.O. Ritchie, P. Yang, A.P. Alivisatos, ACS Appl. Mater. Interfaces **8**, 35523–35533 (2016)
73. F. Krieg, S.T. Ochsenbein, S. Yakunin, S. Ten Brinck, P. Aellen, A. Süess, B. Clerc, D. Guggisberg, O. Nazarenko, Y. Shynkarenko, S. Kumar, C.-J. Shih, I. Infante, M.V. Kovalenko, ACS Energy Lett. **3**, 641–646 (2018)
74. S. Das, A. De, A. Samanta, J. Phys. Chem. Lett. **11**, 1178–1188 (2020)
75. M. Liu, G. Zhong, Y. Yin, J. Miao, K. Li, C. Wang, X. Xu, C. Shen, H. Meng, Adv. Sci. **4**, 1700335 (2017)

76. M. D'Amato, L. Belzane, C. Dabard, M. Silly, G. Patriarche, Q. Glorieux, H. Le Jeannic, E. Lhuillier, A. Bramati, Nano Lett. **23**, 10228–10235 (2023)
77. C.T. Trinh, D.N. Minh, V.L. Nguyen, K.J. Ahn, Y. Kang, K.-G. Lee, APL Mater. **8**, 031102 (2020)
78. L. Chouhan, S. Ito, E.M. Thomas, Y. Takano, S. Ghimire, H. Miyasaka, V. Biju, ACS Nano **15**, 2831–2838 (2021)
79. C. Zhou, Y. Zhong, H. Dong, W. Zheng, J. Tan, Q. Jie, A. Pan, L. Zhang, W. Xie, Nat. Commun. **11**, 329 (2020)
80. C.R. Kagan, C.B. Murray, Nat. Nanotechnol. **10**, 1013–1026 (2015)
81. T.P.T. Nguyen, L.Z. Tan, D. Baranov, J. Chem. Phys. **159**, 204703 (2023)
82. J. Henzie, M. Grünwald, A. Widmer-Cooper, P.L. Geissler, P. Yang, Nat. Mater. **11**, 131–137 (2011)
83. H. Pashaei Adl, S. Gorji, G. Muñoz-Matutano, A.F. Gualdrón-Reyes, I. Suárez, V.S. Chirvony, I. Mora-Seró, J.P. Martínez-Pastor, Adv. Opt. Mater. **11**, 2202497 (2023)
84. M. Biliroglu, G. Findik, J. Mendes, D. Seyitliyev, L. Lei, Q. Dong, Y. Mehta, V.V. Temnov, F. So, K. Gundogdu, Nat. Photonics **16**, 324–329 (2022)
85. G. Rainò, M.A. Becker, M.I. Bodnarchuk, R.F. Mahrt, M.V. Kovalenko, T. Stöferle, Nature **563**, 671–675 (2018)
86. C. Zhu, S.C. Boehme, L.G. Feld, A. Moskalenko, D.N. Dirin, R.F. Mahrt, T. Stöferle, M.I. Bodnarchuk, A.L. Efros, P.C. Sercel, M.V. Kovalenko, G. Rainò, Nature 1–7 (2024)
87. F. Mattiotti, M. Kuno, F. Borgonovi, B. Jankó, G.L. Celardo, Nano Lett. **20**, 7382–7388 (2020)
88. X. Tang, D. Rossi, J. Cheon, D.H. Son, Chem. Mater. **34**, 7181–7189 (2022)
89. S.J. Masson, A. Asenjo-Garcia, Nat. Commun. **13**, 2285 (2022)
90. H. Zhao, Y. Zhao, Y. Song, M. Zhou, W. Lv, L. Tao, Y. Feng, B. Song, Y. Ma, J. Zhang, J. Xiao, Y. Wang, D.-H. Lien, M. Amani, H. Kim, X. Chen, Z. Wu, Z. Ni, P. Wang, Y. Shi, H. Ma, X. Zhang, J.-B. Xu, A. Troisi, A. Javey, X. Wang, Nat. Commun. **10**, 5589 (2019)
91. J. Yang, X. Wen, H. Xia, R. Sheng, Q. Ma, J. Kim, P. Tapping, T. Harada, T.W. Kee, F. Huang, Y.-B. Cheng, M. Green, A. Ho-Baillie, S. Huang, S. Shrestha, R. Patterson, G. Conibeer, Nat. Commun. **8**, 14120 (2017)
92. X.-Y. Zhu, V. Podzorov, J. Phys. Chem. Lett. **6**, 4758–4761 (2015)
93. E.S. Muckley, R. Vasudevan, B.G. Sumpter, R.C. Advincula, I.N. Ivanov, MACS Appl. Mater. Interfaces. **15**, 2329–2340 (2023)
94. W. Choi, R.C. Advincula, H.F. Wu, Y. Jiang, MRS Commun. **13**, 714–724 (2023)
95. G. Zhou, W. Chu, O.V. Prezhdo, ACS Energy Lett. **5**, 1930–1938 (2020)
96. M. Srivastava, J.M. Howard, T. Gong, M. Rebello Sousa Dias, M.S. Leite, J. Phys. Chem. Lett. **12**, 7866–7877 (2021)
97. A.M. Bran, S. Cox, O. Schilter, C. Baldassari, A.D. White, P. Schwaller, Nat. Mach. Intell. **6**, 525–535 (2024)
98. Z. Li, M.A. Najeeb, L. Alves, A.Z. Sherman, V. Shekar, P. Cruz Parrilla, I.M. Pendleton, W. Wang, P.W. Nega, M. Zeller, J. Schrier, A.J. Norquist, E.M. Chan, Chem. Mater. **32**, 5650–5663 (2020)
99. K. Higgins, S.M. Valleti, M. Ziatdinov, S.V. Kalinin, M. Ahmadi, ACS Energy Lett. **5**, 3426–3436 (2020)